Food Science of Animal Products

Research Article

Molecular docking and density functional theory (DFT) studies on the conversion of linoleic acid into fatty acid metabolites by *Lactiplantibacillus plantarum* 12-3

Tariq Aziz[1], Muhammad Naveed[2], Muhammad Aqib Shabbir[2], Abid Sarwar[1], Jasra Naseeb[1], Zhennai Yang[1] ✉

[1] *Key Laboratory of Geriatric Nutrition and Health of Ministry of Education, Beijing Engineering and Technology Research Center of Food Additives, Beijing Advanced Innovation Center for Food Nutrition and Human Health, Beijing Technology and Business University, Beijing 100048, China*

[2] *Department of Biotechnology, Faculty of Life Sciences, University of Central Punjab, Lahore 54590, Pakistan*

✉Address correspondence to Zhennai Yang, yangzhennai@th.btbu.edu.cn

Received: June 18, 2023; Revised: July 5, 2023; Accepted: July 12, 2023

Abstract: The aim of this study was to evaluate the competency of *Lactiplantibacillus plantarum* 12-3 isolated from Tibetan kefir grains that how it converts linoleic acid (LA) into fatty acid metabolites and what are the main reactions involved in it. Also, we scrutinize the enzymes involved in this study via density functional theory (DFT) and *in silico* approaches. The taxonomic identity was performed using average nucleotide identity (ANI) analysis and to investigate its genome properties using the rapid annotations using subsystems technology (RAST) annotation service. After eliminating plasmid sequences to focus on core genomic information, ANI analysis was performed using the JSpecies Web Server. The results verified *L. plantarum* 12-3's categorization as a member of the *L. plantarum* species, demonstrating good conservation and taxonomic relatedness. Heatmapper was used to visualize the ANI data clustering and heatmap, allowing the discovery of closely related strains within *L. plantarum*. RAST annotation of the genome revealed functional subsystems as well as metabolic pathways, cellular activities, and virulence factors. Several routes of future research might be pursued to further investigate the possible applications and distinctive properties of the *L. plantarum* 12-3 strain. To begin, comparative genomics studies with other *L. plantarum* strains would provide a better knowledge of the strain's distinctive genetic variants and evolutionary adaptations. This may give light on its applicability for a variety of industrial uses, including food fermentation and probiotics.

Keywords: molecular docking; linoleic acid; density functional theory; isomerization; reduction; dehydrogenation

Citation: T. Aziz, M. Naveed, M. A. Shabbir, et al., Molecular docking and density functional theory (DFT) studies on the conversion of linoleic acid into fatty acid metabolites by *Lactiplantibacillus plantarum* 12-3, Food Sci. Anim. Prod. 1 (2023) 9240024. https://doi.org/10.26599/FSAP.2023.9240024.

1 Introduction

Gut microbiome has a major role in regulating a number of host-cell metabolic processes, the most notable of which are lipid metabolism, glucose metabolism and homeostasis[1–3]. Certain metabolites, such as lipid metabolites, and signaling molecules produced by intestinal microflora play important roles in boosting up human immunity and function in the host, maintaining a healthy gut-brain-liver axis, and preventing off conditions like inflammatory bowel disease (IBD) and obesity caused by microbial dysbiosis[3–6]. Among the gut microbiome, lactic acid bacteria (LAB) have a long history of use in food processing with a generally regarded as safe (GRAS) status, and they are generally known for many beneficial health effects[7–9]. LAB can produce various antimicrobial compounds including acetic acid, phenyl lactic acid, cyclic dipeptide, 3-hydroxy fatty acids, peptides, etc[10–13]. Many studies have also shown that LAB can convert polyunsaturated fatty acids (PUFAs) like linoleic acid (LA) into various bioactive fatty acid metabolites with non-toxicity to the bacteria[14–18]. Several researches proved the strong linkage between the lipid metabolites and human health[19]. Albouery et al.[20] reported that these metabolites play a crucial role in influencing age-related variations and distribution patterns in lipid metabolism. Based on the aforementioned investigations, it appears that understanding and modulating the lipid metabolic pathways of gut microbiota is an important approach for the improvement of human health[20].

Among the genus of *Lactobacillus*, *Lactiplantibacillus* is widely present in plants, fermented foods, meat, juices, and the digestive systems of humans and animals[15]. *Lactiplantibacillus plantarum* is commonly found in the human digestive tract, and it can be used as a starter in animal diets and as a dietary supplement for humans[21]. In our previous studies[14–21], we demonstrated that how *L. plantarum* 12-3 isolated from Tibetan kefir was capable of converting LA into conjugated linoleic acid (CLA) and different fatty acid metabolites in the medium supplemented with LA ranging from 1% to 10%, but the mechanism of conversion was unclear. Recent research has found that some gut bacteria species and their metabolites might alter lipid metabolism, including lipid production, absorption, and storage, possibly influencing overall metabolic health and the development of diseases such as obesity

and cardiovascular disease[22]. With the recent advances and availability of reasonable sequencing technologies and software development in genomics and metagenomics, the present study was carried out to determine the whole genome sequence of *L. plantarum* 12-3, and analyze genes related to lipid metabolism. Characterization of the main reactions involved in conversion of LA to different fatty acid metabolites, and the main enzymes responsible for these reactions was performed via blasting the whole genome sequence of the strain, molecular docking, and density functional theory (DFT) studies. The present study provides further understanding on the lipid metabolism in *L. plantarum* that plays a part in exerting its beneficial health effects.

2 Materials and methods

2.1 Bacterial strain and growth condition

L. plantarum 12-3 isolated from Tibetan kefir was kept as a frozen stock at –80 ℃. The strain was repeatedly activated for three times at 37 ℃ in MRS medium (Beijing Aoboxing Co., Ltd.) containing 2.0% glucose, 1.0% meat extract, 1.0% tryptone, 0.5% yeast extract, 0.1% Tween-80, 0.2% K_2HPO_4, 0.5% sodium acetate, 0.2% diammonium citrate, 0.02% $MgSO_4{\cdot}7H_2O$ and 0.005% $MnSO_4{\cdot}H_2O$. Distilled water was used as solvent for dissolving medium components, and the medium was adjusted to pH 5.5 and sterilized at 121 ℃ for 15 min[14,23].

2.2 Whole genome sequencing of *L. plantarum* 12-3

L. plantarum 12-3 was incubate at 37 ℃ for 24 h, and then centrifuged to collect cells (4 ℃, 12 000 × *g*, 10 min), then, after DNA extraction in Shanghai Majorbio Bio-Pharm Tech Co., Ltd., (China), Illumina HiSeq × 10 sequencing platform at 2 × 150 paired-end reads were used for sequencing analysis. For *de novo* genome assembly, clean reads for each strain were assembled using SOAPdenovo 2. After removing low-quality data obtained by the sequencing platform, Glimmer was used to predict coding sequences and GC content.

2.3 Genome annotation and features exploration

The rapid annotations using subsystems technology (RAST) annotation server was used to perform genome annotation. The genomic DNA sequence was acquired in FASTA format. The sequence can be acquired using PacBio or Illumina, two sequencing methods. The genomic sequence's FASTA file was uploaded to the RAST annotation system. The server can be obtained via https://rast.nmpdr.org/. The sequence can be submitted using the server's web interface, albeit a user account might be necessary. The RAST server examined the provided sequence to find probable protein-coding genes. For gene prediction, RAST uses algorithms like Glimmer and Prodigal. The start and stop points of the open reading frames (ORFs) were identified.

The found genes functions were determined by comparing their protein sequences to databases such as Clusters of Orthologous Groups (COG), Pfam, and the SEED database. RAST assigns functional annotations to predicted genes using a combination of homology-based searches, hidden Markov models (HMMs), and other bioinformatics methods. Based on their annotations, RAST further classified the predicted genes into functional subsystems. Subsystems are groupings of genes that collaborate to carry out certain biological functions. The gene annotations were compared to predefined subsystems in the SEED database to make the allocations.

2.4 Phylogenetic ANI and clustering studies

An investigation of the average nucleotide identity (ANI) of *L. plantarum* strains was done in order to confirm the taxonomic identity of the *L. plantarum* 12-3 strain. The JSpecies Web Server, which is free and accessible at http://jspecies.ribohost.com/jspeciesws, was used to do ANI analysis after plasmid removal. Heatmapper (http://www.heatmapper.ca) was used to produce a clustering and heatmap.

2.5 Molecular docking and DFT studies

The entire sequencing of *L. plantarum* 12-3 genome allowed for the identification of the conversion of LA and its fatty acid metabolites (GCA_003641185.1). To acquire the primary amino acid sequence, *in silico* analysis was employed to evaluate the tertiary protein structure and interaction of LA with *L. plantarum* 12-3 (https://www.ncbi.nlm/nih.gov/assembly/GCA_003641185.1). Then using the SWISS-MODEL that is a fully automated protein structure homology modeling server. The protein module was visualized by protein visualizing program Discovery Studio 3.5[24]. The LA molecule was drawn in molecular operating environment (MOE) assigned with proper 2D orientation, then minimized energy of using Avogadro[24] with MMFF94 force field. Docking calculation was applied with the MOE[25]. The active site was predicted by different softwares[26–27].

Calculations were run based on DFT with unconstrained spin using the DMol3 module. Generalized gradient approximation (GGA) with the Becke3-Lee-Yang-parr (B3LYP) level using the 6-311G** basis set were applied. The chemical reactivity parameters computed for AO and HERA are as follows: S represents softness (measurement of molecules' stability), η represents hardness (reverse of softness), DM represents dipolmoment, chemical potential, χ represents electronegativity (grabbing-electrons-power), $\mu-$ and $\mu+$ represents electronic affinity transfer and accept, respectively, $\omega-$ and $\omega+$ represents molecule suitability for providing and gaining an electron, respectively, ω_i represents electrophilicity index (evaluating the relative strengths of electron donors and acceptors), $\Delta N_{max} = \chi/2\eta$ (highest amount of electrons that can be exchanged in a chemical reaction), I represents ionization-potential, and A represents electron affinity.

3 Results and discussion

3.1 Theoretical assay

The novel *L. plantarum* 12-3 genome was assessed further via DFT using B3LYP/ 6-311G**++ used for computational study for the five of the fatty acids derived from LA. Figure 1 showed that the optimized high occupied molecular orbital (HOMO), low unoccupied molecular orbital (LUMO) and molecular-electrostatic-potential profile (MEPs) for the tested compounds. The chemical parameters were calculated using equations as reported by Rubab et al.[28].

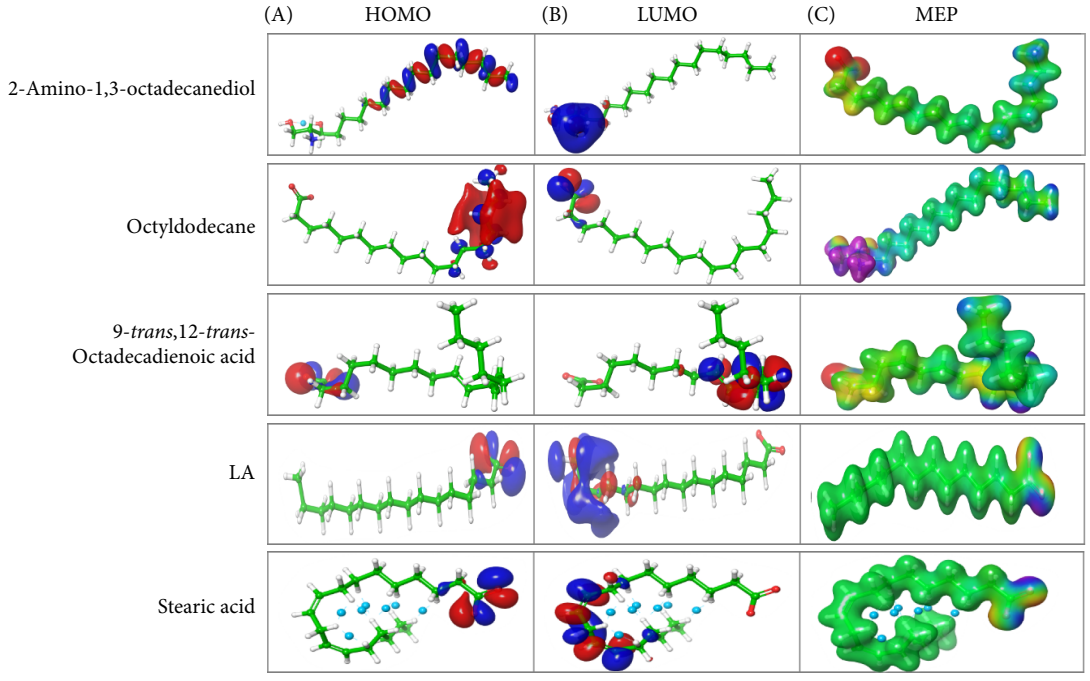

Figure 1 FMOs obtained for AO and HERA (DFT/B3YLB/6-311G**).

3.2 Stability of inter- and intramolecular interaction against kinases: frontier molecular orbitals (FMOs) analysis

HOMO and LUMO are known as "FMOs" and determined by donating/accepting-electrons, respectively, which may determine the route binding of *Lactiplantibacillus* with a LA kinases[27]. Molecule's chemical reactivity and kinetic stability was calculated by FMO gap. Stabilization (inhibitor-surface) was enhanced by increasing the inhibitor's HOMO energy and decreasing the surface's LUMO energy[29].

E_{HOMO} (the energy level of HOMO) in liquid phase is greater than gaseous zone and the components are in descending order as follow 9-*trans*,12-*trans*- octadecadienoic acid, octyldodecane, 2-amino-1,3-octadecanediol, stearic, and LA. The bigger E_{HOMO} value than E_{LUMO}, that imply a greater possibility of losing valance electrons and a stronger desire to donate electrons toward the surface of iron, and more inhibitory potency than gas phase[28–29]. All of the fatty acids studied had HOMOs anchored to the carboxyl group, while the LUMOs were found to be positioned on the aliphatic side. The penetration of the carboxylic centers of LA-kinases by the charge from *Lactiplantibacillus* was indicated by the negative E_{HOMO} and E_{LUMO}.

3.3 Electrostatic potential surface (ESP) efficiency for their absorption effect over kinase

ESP efficiency for their absorption effect over kinase was tested following the method of Raza et al.[32]. The scattering force signifies as blue color and caused to electron-donation-power. Color coded (orange, yellow, red) attractive force associated with electron accepting "–" charge. The green shade indicates a moderately promising future. For inhibitors who have undergone tests of ESP (Figure 1). The negative charges were distributed as follows: 2-amino-1,3-octadecanediol, 9-*trans*,12-*trans*- octadecadienoic acid, linoleic, stearic acid, and octadecadienoic. ESP surface's colour changes indicated variation for their values.

3.4 Phylogenetic ANI and clustering studies

To validate the taxonomic identity of the *L. plantarum* 12-3 strain, ANI analysis was carried out. For this analysis, we used the JSpecies Web Server, a free online application accessible at http://jspecies.ribohost.com/jspeciesws. Plasmid sequences were taken out to concentrate on the main genomic information before ANI analysis.

The level of similarity between the *L. plantarum* 12-3 strain and other recognized *L. plantarum* strains was determined using the ANI analysis. The *L. plantarum* 12-3 strain is undoubtedly a member of the *L. plantarum* species, according to the data, which also showed a high level of conservation and taxonomic relatedness. Heatmapper, an online program available at http://www.heatmapper.ca was used to display the clustering and heatmap of the ANI data. The heatmap gave a visual depiction of how genetically similar the *L. plantarum* 12-3 strain and the reference strains are to one another. The identification of closely related strains within the *L. plantarum* species was made possible by clustering of strains based on their ANI values. The JSpecies Web Server's ANI analysis and Heatmapper's display of the results gave us important new understandings about the taxonomic identification and genetic relatedness of the *L. plantarum* 12-3 strain. These results contributed to a better understanding of the genetic background of *L. plantarum* 12-3 within the *L. plantarum* species and support the designation of *L. plantarum* 12-3 as a member of the *L. plantarum* species[30–31].The heatmap for ANI clustering was given in Figure 2.

3.5 Genome annotation and features exploration

The RAST annotation service was used to annotate the target organism's genome. The annotation procedure revealed useful information about the functional content of the genome and

highlighted numerous subsystem statistics and genomic traits. Based on their annotations, The Pathosystems Resource Integration Center (PATRIC) annotation server grouped the predicted genes into functional subsystems[30–31]. The distribution of genes across distinct functional categories was shown by the subsystem statistics. The subsystem statistics and subsystem features were shown in Figure 3.

3.6 Δ*G* values

The stability index and interaction between $HOMO_{inhibitor}$ and $LUMO_{kinase}$ were stabilized indirectly with energy gap. The Δ*G* related directly with the electrophile (soft/hard) [33–34]. The Δ*G* values are nearly equal and arranged as 9-*trans*,12-*trans*- octadecadienoic acid, octyldodecane, 2-amino-1,3-octadecanediol, stearic, and LA. LA showed most promising softanse against all tested fatty acids (Table 1). We examined the amount of the electrons transfer from the inhibitor to the kinase by calculate the "$\mu-$" and "$\omega-$"[33–36] (Table 1).

3.7 LA's metabolite conversion by *L. plantarum in silico*

Various enzymes are responsible for the conversion of LA to different metabolites in *L. plantarum* 12-3 and the conversion is done via different reactions. The most vital reactions for LA biotransformation to fatty acid analogues using *L. plantarum* 12-3 are isomerization, dehydrogenation, and reduction. Three assumed enzymes were detected by the method of Hu et al.[37] (GCA_003641145.1) as represented in Figure 4.

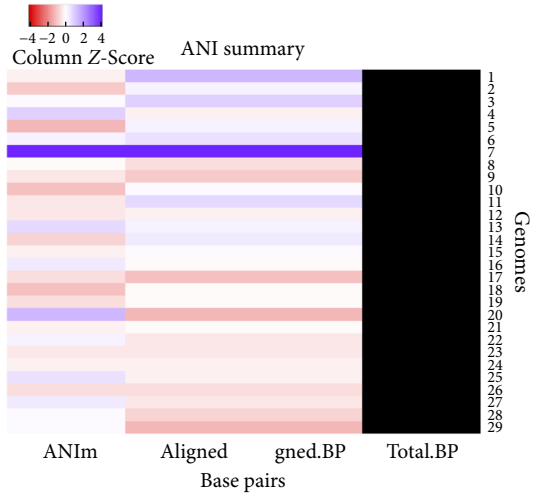

Figure 2 Clustering heatmap of the aligned base pairs and ANI.

3.8 Dehydrogenation

In silico, the dehydrogenase enzyme plays a circular role in this dehydrogenation process. The active site's amino acid residues which involved in this dehydrogenation mechanism including Asp11, Cys14, Gln15, Thr18, Glu145, Asn146, Tyr147, Mse149, and Lys150. All tested compounds successfully docked into the dehydrogenase binding pocket. The COOH groups for tested fatty acids (stearic acid, 9-*trans*,12-*trans*-octadecadienoic acid, 2-amino-1,3-octadecanediol, octyldodecane and LA) interacted respectively with vital amino acids of active site through key-lock mode as: Gln245 & Arg189, Gly214 & Gln215, Arg189, Lys188, Tyr248 & Arg189, respectively (Figure 5).

In silico prediction key-lock theory postulated that all isolated fatty acids capped the dehydrogenase-binding-pocket by formation of the H-bonds between the OH for the acidic group of fatty acids and amino acids of the enzymatic binding pocket. H-interaction is vital for the dehydrogenation biotransformation as it accelerates the flavin adenine dinucleotide (FAD) reaction with substrate. Subsequently, the enzyme's mechanistic process, FAD is converted into FADH2, which forms a new double bond in LA as the substrate. In this instance, dehydrogenation is FAD-dependent[37–38]. The binding pocket for tested compounds arranged as LA, stearic acid, 2-amino-1,3-octadecanediol, 9-*trans*,12-*trans*-octadecadienoic acid, and octyldodecane (Table 2).

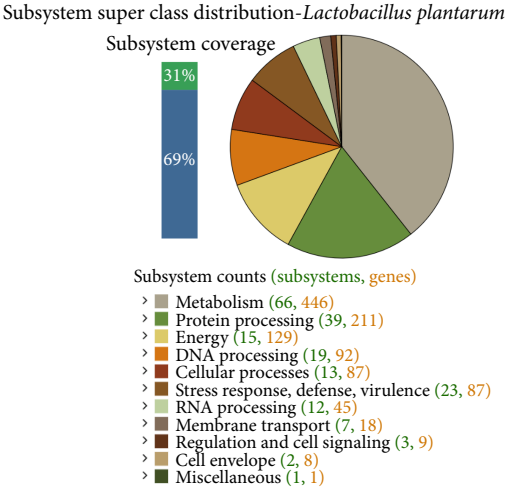

Figure 3 The subsystem statistics and genome features explored by PATRIC annotation server.

Table 1 Isolated fatty acids reactivity parameters at DFT/B3YLB/6-311G**++.

Fatty acids	HOMO	LUMO	Δ*G*	DM	*η*	*S*	*χ*	*I*	*A*	EP	ω_i	*μ*+	*μ*−	*ω*−	*ω*+	*ΔEBD*	N_{max}
2-Amino-1,3-octadecanediol	−0.07	−0.13	0.6	36.37	0.06	16.12	0.06	−0.01	−0.13	−0.07	0.03	0.10	0.04	0.01	0.03	−0.02	−0.55
Octyldodecane	−0.06	−0.16	0.1	32.07	0.04	25.19	0.04	−0.01	−0.09	−0.05	0.02	0.07	0.03	0.01	0.02	−0.01	−0.58
9-*trans*,12-*trans*-Octadecadienoic acid	−0.08	−0.12	0.4	35.13	0.06	16.51	0.06	−0.01	−0.13	−0.07	0.03	0.10	0.04	0.01	0.03	−0.02	−0.57
LA	−0.09	−0.13	0.4	33.21	0.06	15.71	0.06	−0.01	−0.14	−0.07	0.03	0.10	0.04	0.01	0.03	−0.02	−0.57
Stearic acid	−0.06	−0.18	0.2	24.58	0.03	28.58	0.03	−0.01	−0.08	−0.04	0.02	0.06	0.02	0.01	0.02	−0.01	−0.59

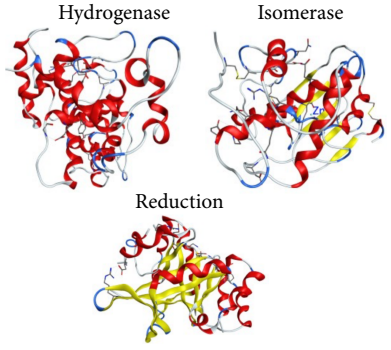

Figure 4 Tertiary structure of three assumed enzymes including the transformation of LA to LA analogues.

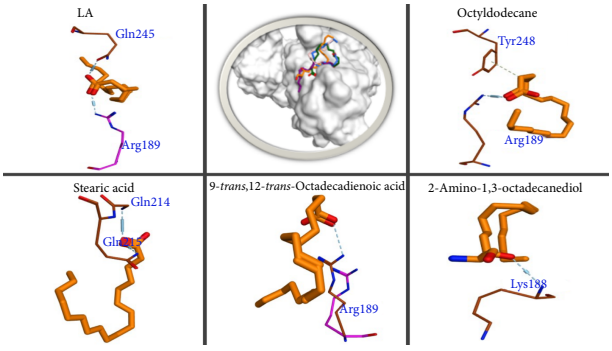

Figure 5 *In silico* analysis of LA with *L. plantarum* 12-3 dehydrogenase enzyme (MOE tool).

Table 2 The binding pocket for tested compounds.

	Fatty acids	S	RMSD	E_conf	E_place	E_score1
1LBU	LA	−9.15	2.12	63.17	−92.43	−11.36
	2-Amino-1,3-octadecanediol	−8.77	1.75	65.39	−96.51	−10.80
	Octyldodecane	−8.39	1.21	−16.02	−100.50	−9.58
	9-*trans*,12-*trans*-Octadecadienoic acid	−8.27	3.11	59.08	−70.34	−9.50
	Stearic acid	−8.20	1.28	−14.74	−74.47	−9.14
3BKH	LA	−18.88	5.72	59.38	−59.86	−9.11
	2-Amino-1,3-octadecanediol	−13.78	3.46	−12.08	−49.18	−9.53
	Octyldodecane	−8.63	3.84	−8.47	−59.95	−11.46
	9-*trans*,12-*trans*-Octadecadienoic Acid	−10.17	3.54	−11.94	−45.70	−9.37
	Stearic acid	−16.56	2.66	−11.52	−36.27	−9.05
4J9J	LA	−6.62	1.80	61.89	−49.84	−12.30
	2-Amino-1,3-octadecanediol	−7.03	1.21	−14.76	−49.60	−11.35
	Octyldodecane	−6.67	2.03	−14.35	−43.55	−12.57
	9-*trans*,12-*trans*-Octadecadienoic acid	−6.77	1.35	−20.12	−39.58	−11.18
	Stearic acid	−6.63	1.84	−14.13	−38.49	−11.58

Note: S represents score, RMSD represents root mean square deviation, E_conf represents configuration energy, E_place represents energy placement, E_score1 represents energy score.

3.9 Isomerization

In silico analysis demonstrated that the linoleate-isomerase catalyzes the biotransformation of the *Z*,*Z* to *E*,*Z* of LA using *L. plantarum* 12-3 (Figure 6). Amino acid residues are Arg138, Asn143, Val146, Gly147, Gly148, Ala149, Asn151, Ser152, Arg153, His154, Tyr156, His158, Asp161, Glu183, Leu185, Tyr189, His192, His195, His197, Gly201, Asp202, and ZN214. The linoleate-isomerase is nicotinamide adenine dinucleotide phosphate (NADPH) dependent which converted the LA double bond into a single bond, and reversibly the inversion of configuration tack place (Figure 4). All compound capped active site by chelation with Zn metal ions to form octahedral stable shape[39–40]. LA showed highest binding efficiency (−9.15 kcal/mol). The binding efficiency against LA-isomerase was arranged as 2-amino-1,3-octadecanediol, octyldodecane, 9-*trans*,12-*trans*-octadecadienoic acid, and stearic acid.

3.10 Reduction

L-Glutathione and trypanothione are two possible nucleophiles found all living cells in *L. plantarum* 12-3, that reduce LA into two different compounds with a single bond, as 6-/9-octadecenoic acids. The reduction mechanism well known as NADPH dependent (Figure 7). Glutathione and trypanothione nucleophiles, in the first

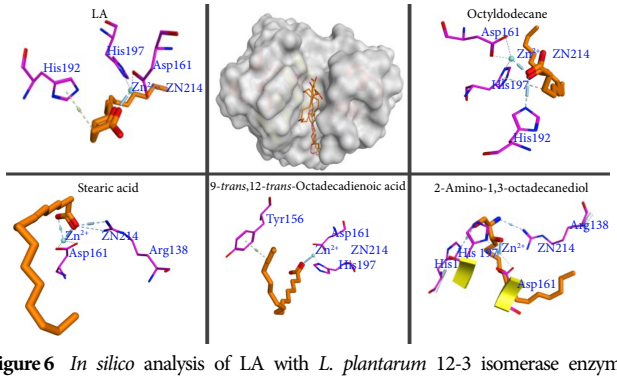

Figure 6 *In silico* analysis of LA with *L. plantarum* 12-3 isomerase enzyme (MOE tool).

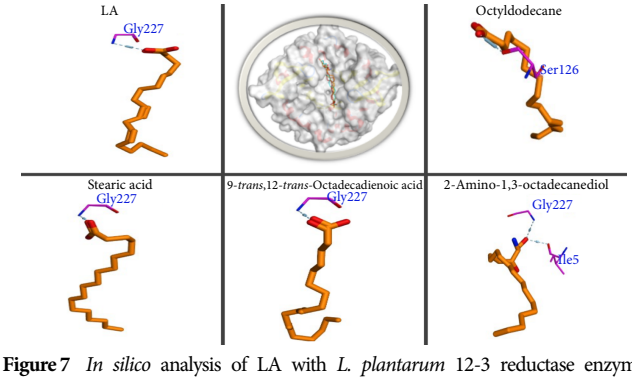

Figure 7 *In silico* analysis of LA with *L. plantarum* 12-3 reductase enzyme (MOE tool).

stage formed a complex with LA, and NADPH's action on LA in the second step causes reduction. Amino acid residues are Ile5, Ile6, Asn7, Thr8, Ala9, Ala10, Ala32, Ile33, Asp34, Ala35, Lys36, Phe45, Thr46, Tyr47, Ser48, Gly49, Lys50, Leu73, Leu74, Ala75, Ser76, Ser105, Gly106, Gly107, Ala108, Phe114, Ser126, Ile127, Asn128, Thr129, Ala130, Ala153, Val155, Tyr168, Ser169, Leu194, Thr196, Ser226, Gly227, Gly228, Ala229, and Phe235. From the induced fit docking into the active site residues, we can see two H-bonds formed between carboxy group for LA and His-3 and Glu145. From formed important H-bonds with LA, that serving in the catalysis of the substrate. 2-Amino-1,3-octadecanediol most potent binding activity while other compounds showed nearly the same binding energy about 6.6 kcal/mol.

4 Conclusion

The main reactions involved in converting LA into various fatty acid metabolites by *L. plantarum* 12-3 were dehydrogenation, isomerization and reduction as confirmed by molecular docking and DFT studies. The presence of genes involved in several metabolic processes, such as carbohydrate metabolism, amino acid metabolism, lipid metabolism, and other critical metabolic functions, was shown by the subsystem statistics. These findings point to the target organism's metabolic adaptability. Furthermore, the annotation results revealed information about unique genomic traits. These characteristics included the discovery of genes involved in a variety of biological activities, such as DNA replication, transcription, translation, and cell wall construction. Furthermore, the annotation highlighted the presence of genes associated with stress response, transport systems, and virulence factors, indicating the organism's adaptability and potential toxicity. These metabolites are of very much importance and can be used for further studies. The activities and bio functional properties of these metabolites can further be confirmed via *in vivo* and *in vitro* approaches.

Conflict of interest

The authors declare no conflict of interest.

Acknowledgements

This work was supported by the National Natural Science Foundation of China (32272296).

References

[1] T. Aziz, S. Abid, D. Zubaida, et al., Conjugated fatty acids (CFAS) production via various bacterial strains and their applications: a review, J. Chil. Chem. Soc. 67 (2022) 5445–5452. https://doi.org/10.4067/S0717-97072022000105445.

[2] M. Zhang, X. N. Hao, A. Tariq, et al., Exopolysaccharides from *Lactobacillus plantarum* YW11 improve immune response and ameliorate inflammatory bowel disease symptoms, Acta Biochim. Pol. 67(4) (2020) 485–493. https://doi.org/10.18388/abp.2020_5371.

[3] J. L. Sonnenburg, F. Bäckhed, Diet-microbiota interactions as moderators of human metabolism, Nature 535 (2016) 56–64. https://doi.org/10.1038/nature18846.

[4] M. Schoeler, R. Caesar, Dietary lipids, gut microbiota and lipid metabolism. Rev. Endocr. Metab. Dis. 20 (2019) 461–472. https://doi.org/10.1007/s11154-019-09512-0.

[5] S. Z. Wang, Y. J. Yu, K. Adeli, Role of gut microbiota in neuroendocrine regulation of carbohydrate and lipid metabolism via the microbiota-gut-brain-liver axis, Microorganisms 8 (2020) 527. https://doi.org/10.3390/microorganisms8040527.

[6] E. Amabebe, F. O. Robert, T. Agbalalah, et al., Microbial dysbiosis-induced obesity: role of gut microbiota in homoeostasis of energy metabolism, Br. J. Nut. 123 (2020) 1127–1137. https://doi.org/10.1017/S0007114520000380.

[7] A. Sarwar, A. Tariq, U. D. Jalal, et al., Pros of lactic acid bacteria in microbiology: a review, Biomed. Lett. 4 (2018) 59–66.

[8] T. Aziz, A. Sarwar, M. Naveed, Bio-molecular analysis of selected food derived *Lactiplantibacillus* strains for CLA production reveals possibly a complex mechanism, Food Res. Int. 154 (2022) 111031. https://doi.org/10.1016/j.foodres.2022.111031.

[9] J. J. Jeong, H. J. Park, M. G. Cha, et al., The *Lactobacillus* as a probiotic: focusing on liver diseases, Microorganisms 10 (2022) 288. https://doi.org/10.3390/microorganisms10020288.

[10] M. Atanassova, Y. Choiset, M. Dalgalarrondo, et al., Isolation and partial biochemical characterization of a proteinaceous anti-bacteria and anti-yeast compound produced by *Lactobacillus paracasei* subsp. *paracasei* strain M3, Int. J. Food Microbiol. 87 (2003) 63–73. https://doi.org/10.1016/s0168-1605(03)00054-0.

[11] A. Broberg, K. Jacobsson, K. Ström, et al., Metabolite profiles of lactic acid bacteria in grass silage, Appl. Environ. Microbiol. 73 (2007) 5547–5552. https://doi.org/10.1128/AEM.02939-06.

[12] P. Lavermicocca, F. Valerio, A. Evidente, et al., Purification and characterization of novel antifungal compounds from the sourdough *Lactobacillus plantarum* strain 21B, Appl. Environ. Microbiol. 66 (2000) 4084–4090. https://doi.org/10.1128/AEM.66.9.4084-4090.2000.

[13] E. J. Yang, Y. S. Kim, H. C. Chang, Purification and characterization of antifungal δ-dodecalactone from *Lactobacillus plantarum* AF1 isolated from kimchi, J. Food Prot. 74 (2011) 651–657. https://doi.org/10.4315/0362-028X.JFP-10-512.

[14] T. Aziz, A. Sarwar, J. Ud Din, et al., Biotransformation of linoleic acid into different metabolites by food derived *Lactobacillus plantarum* 12-3 and *in silico* characterization of relevant reactions, Food Res. Int. 147 (2021) 110470. https://doi.org/10.1016/j.foodres.2021.110470.

[15] T. Aziz, M. Naveed, S. I. Makhdoom, et al., Genome investigation and functional annotation of *Lactiplantibacillus plantarum* YW11 revealing streptin and ruminococcin-a as potent nutritive bacteriocins against gut symbiotic pathogens, Molecules 28 (2023) 491. https://doi.org/10.3390/molecules28020491.

[16] T. Aziz, A. Sarwar, M. Fahim, et al., Dose-dependent production of linoleic acid analogues in food derived *Lactobacillus plantarum* K25 and *in silico* characterization of relevant reactions, Acta Biochimica. Polonica. 67 (2020) 123–129. https://doi.org/10.18388/abp.2020_5167.

[17] T. Aziz, A. Sarwar, M. Fahim, et al., Conversion of linoleic acid to different fatty acid metabolites by *Lactobacillus plantarum* 13-3 and *in silico* characterization of the prominent reactions, J. Chil. Chem. Soc. 65 (2020) 4879–4884. https://doi.org/10.4067/s0717-97072020000204879.

[18] T. Aziz, A. Sarwar, A. D. Sam, et al., Production of linoleic acid metabolites by different probiotic strains of *Lactobacillus plantarum*, Prog. Nutr. 21 (2019) 693–701. https://doi.org/10.23751/pn.v21i3.8573.

[19] J. Rodríguez-Carrio, N. Salazar, A. Margolles, et al., Free fatty acids profiles are related to gut microbiota signatures and short-chain fatty acids, Front. Immunol. 8 (2017) 823. https://doi.org/10.3389/fimmu.2017.00823.

[20] M. Albouery, B. Buteau, S. Grégoire, et al., Age-related changes in the gut microbiota modify brain lipid composition, Frontiers in Cellular and Infection Microbiology 9 (2020) 444. https://doi.org/10.3389/fcimb.2019.00444.

[21] M. Kleerebezem, J. Boekhorst, R. V. Kranenburg, et al., Complete genome sequence of *Lactobacillus plantarum* WCFS1, PNAS

100(4) (2003) 1990–1995. https://doi.org/10.1073/pnas.0337704100.

[22] J. Aron-Wisnewsky, M. V. Warmbrunn, M. Nieuwdorp, et al., Metabolism and metabolic disorders and the microbiome: the intestinal microbiota associated with obesity, lipid metabolism, and metabolic health-pathophysiology and therapeutic strategies, Gastroenterology 160 (2021) 573–599. https://doi.org/10.1053/j.gastro.2020.10.057.

[23] T. Aziz, M. Naveed, A. Sarwar, et al., Functional annotation of *Lactiplantibacillus plantarum* 13-3 as a potential starter probiotic involved in the food safety of fermented products, Molecules 27 (2022) 5399. https://doi.org/10.3390/molecules27175399.

[24] S. Sharma, P. Kumar, R. Chandra, Applications of BIOVIA materials studio, LAMMPS, and GROMACS in various fields of science and engineering, in: S. Sharma (Eds.), Molecular dynamics simulation of nanocomposites using biovia materials studio, lammps and gromacs, 2019, pp. 329–341. https://doi.org/10.1016/B978-0-12-816954-4.00007-3.

[25] G. M. Morris, R. Huey, W. Lindstrom, et al., AutoDock4 and AutoDockTools4: automated docking with selective receptor flexibility, J. Comput. Chem. 30 (2009) 2785–2791. https://doi.org/10.1002/jcc.21256.

[26] J. A. Bell, Y. Cao, J. R. Gunn, et al., PrimeX and the schrödinger computational chemistry suite of programs, in: Crystallography of biological macromolecules, Second Online Edition, 2012, Part 18. https://doi.org/10.1107/97809553602060000864.

[27] R. De Cario, E. Sticchi, L. Lucarini, et al., Role of TGFBR1 and TGFBR2 genetic variants in Marfan syndrome, J. Vasc. Surg. 68 (2018) 225–233.e5. https://doi.org/10.1016/j.jvs.2017.04.071.

[28] S. L. Rubab, A. R. Raza, B. Nisar, et al., Synthesis, crystal structure, DFT calculations, hirshfeld surface analysis and *in silico* drug-target profiling of (*R*)-2-(2-(1,3-dioxoisoindolin-2-yl)propanamido)benzoic acid methyl ester, Molecules 28 (2023) 4375. https://doi.org/10.3390/molecules28114375.

[29] C. Deslouis, B. Tribollet, G. Mengoli, et al., Electrochemical behaviour of copper in neutral aerated chloride solution. I. Steady-state investigation, J. Appl. Electrochem. 18 (1988) 374–383. https://doi.org/10.1007/BF01093751.

[30] T. Aziz, M. Naveed, K. Jabeen, et al., Integrated genome based evaluation of safety and probiotic characteristics of *Lactiplantibacillus plantarum* YW11 isolated from Tibetan kefir, Front. Microbiol. 20 (2023) 1157615. https://doi.org/10.3389/fmicb.2023.1157615.

[31] T. Aziz, M. Naveed, M. A. Shabbir, et al., Comparative genomics of food-derived probiotic *Lactiplantibacillus plantarum* K25 reveals its hidden potential, compactness, and efficiency, Front. Microbiol. 14 (2023). https://doi.org/10.3389/fmicb.2023.1214478.

[32] A. R. Raza, S. L. Rubab, M. Ashfaq, et al., Evaluation of antimicrobial, anticholinesterase potential of indole derivatives and unexpectedly synthesized novel benzodiazine: characterization, DFT and hirshfeld charge analysis, Molecules 28 (2023) 5024. https://doi.org/10.3390/molecules28135024.

[33] S. S. Alarfaji, F. Rasool, B. Iqbal, et al., *In silico* designing of thieno[2,3-*b*]thiophene core-based highly conjugated, fused-ring, near-infrared sensitive non-fullerene acceptors for organic solar cells, ACS Omega. 27 (2023) 4767–4781. https://doi.org/10.1021/acsomega.2c06877.

[34] K. Azgaou, M. Damej, S. El Hajjaji, et al., Synthesis and characterization of *N*-(2-aminophenyl)-2-(5-methyl-1*H*-pyrazol-3-yl) acetamide (AMPA) and its use as a corrosion inhibitor for C38 steel in 1 M HCl. Experimental and theoretical study, J. Mol. Struct. 1266 (2022) 133451. https://doi.org/10.1016/j.molstruc.2022.133451.

[35] L. Toukal, D. Belfennache, M. Foudia, et al., Inhibitory power of *N,N*-(1,4-phenylene) bis(1-(4-nitrophenyl)methanimine) and the effect of the addition of potassium iodide on the corrosion inhibition of XC70 steel in HCl medium: theoretical and experimental studies, Int. J. Corros. Scale Inhib. 11 (2022) 438–464. https://doi.org/10.17675/2305-6894-2022-11-1-26.

[36] K. Chkirate, K. Azgaou, H. Elmsellem, et al., Corrosion inhibition potential of 2-[(5-methylpyrazol-3-yl)methyl] benzimidazole against carbon steel corrosion in 1 M HCl solution: combining experimental and theoretical studies, J. Mol. Liq. 321 (2021) 114750. https://doi.org/10.1016/j.molliq.2020.114750.

[37] P. Hu, U. Ali, T. Aziz, et al., Investigating the effect on biogenic amines, nitrite, and *N*-nitrosamine degradation in cultured sausage ripening through inoculation of *Staphylococcus xylosus* and lactic acid bacteria, Front. Microbiol. 9 (2023) 1156413. https://doi.org/10.3389/fmicb.2023.1156413.

[38] P. Hu, U. Ali, J. Wang, et al., Comparative study on physicochemical properties, microbial composition and the volatile component of different light flavor Daqu, Food Sci. Nutr. (2023) 1–14. https://doi.org/10.1002/fsn3.3476.

[39] T. Aziz, A. A. Khan, A. Tzora, et al., I. Dietary implications of the bidirectional relationship between the gut microflora and inflammatory diseases with special emphasis on irritable bowel disease: current and future perspective, Nutrients 15 (2023) 2956. https://doi.org/10.3390/nu15132956.

[40] J. Wang, T. Aziz, R. Bai, et al., Dynamic change of bacterial diversity, metabolic pathways, and flavor during ripening of the Chinese fermented sausage, Front. Microbiol. 13 (2022) 990606. https://doi.org/10.3389/fmicb.2022.990606.